

## Time correlation inside a laser pulse

I. A. Ivanov<sup>1,2,\*</sup>, A. S. Kheifets<sup>1,†</sup> and Kyung Taec Kim<sup>2,3,‡</sup>

<sup>1</sup>*Research School of Physics, The Australian National University, Canberra ACT 2600, Australia*

<sup>2</sup>*Center for Relativistic Laser Science, Institute for Basic Science (IBS), Gwangju 61005, Republic of Korea*

<sup>3</sup>*Department of Physics and Photon Science, GIST, Gwangju 61005, Korea*

 (Received 1 December 2019; revised manuscript received 5 December 2019; accepted 20 March 2020; published 15 April 2020)

Looking inside a laser pulse by detecting an instantaneous ionization rate (IIR) has been a useful instrument for characterizing subcycle ionization dynamics [Phys. Rev. A **64**, 013409 (2001)]. However, this instrument relies entirely on IIR being a deterministic function of time. By introducing an IIR operator and studying its autocorrelation function, we show that electron ionization dynamics is more complex and the ionization rate depends on the “prehistory,” i.e., the IIRs at the two instants of time are, in fact, correlated. The pattern of this correlation changes dramatically between the multiphoton and tunneling ionization regimes. These findings have wide implications for strong-field atomic physics and providing new possibilities for quantum local realism tests.

DOI: [10.1103/PhysRevA.101.043407](https://doi.org/10.1103/PhysRevA.101.043407)

### I. INTRODUCTION

A correlation between seemingly unrelated events or quantities is considered as a paradox in science. In quantum physics, examples of such correlations are abundant. The Einstein-Podolsky-Rosen paradox [1] correlates the quantum states of two particles which are miles away and are seemingly not interacting. The Hanbury Brown and Twiss effect [2] correlates (or anticorrelates) the number of photons or massive subatomic [3] or atomic [4] particles coming to two distant detectors. Resolving these paradoxes had a long-lasting effect on fundamental quantum physics [5,6].

Interaction of short and intense laser pulses with matter has been considered a deterministic process fully within the reign of time-resolved quantum mechanics. Interaction of such laser pulses with atoms was described by instantaneous ionization rate (IIR), first introduced in the quasistatic regime of slowly varying laser field [7,8] and then extended to arbitrarily fast ionization processes [9]. The latter generalization allowed a description of a subcycle electron dynamics which played a key role in fundamental processes of high-order harmonic generation and above-threshold ionization [10,11].

The IIR is also used to define the tunneling time as a lag between the instants when the IIR and electric field of the laser pulse are at their respective maxima [12]. For such a definition to be meaningful the IIR should be a well-defined deterministic function of time. In the meantime, a probabilistic treatment of tunneling ionization has been introduced [13] which puts such a definition into question. While the debate on the nature of tunneling ionization and its timing characterization is still open [12–18], we attempt to provide a fresh insight into this problem by performing a time-correlation analysis.

In this work, we employ an autocorrelation function which relates the IIR at the two instants of time. Our present time-correlation analysis shows that the IIR depends on the “prehistory,” i.e., the instantaneous ionization rates at the two instants of time are, in fact, correlated. The pattern of this correlation varies dramatically between the multiphoton and tunneling ionization regimes. We illustrate our findings by considering the hydrogen atom driven by a nearly single-cycle laser pulse with a varying electric field strength which covers a wide range of Keldysh parameters  $\gamma$ . We give a qualitative explanation of the profound change of the correlation pattern between  $\gamma \gg 1$  to  $\gamma \leq 1$  regimes. This explanation rests on the lowest order perturbation theory (LOPT) and the well-known simple man model (SMM) [10,11] for these two regimes, respectively. Our technique allows one to look scrupulously inside the laser pulse, and our findings will be useful for elucidating various subcycle and intracycle interference phenomena.

### II. THEORY

We use the definition of the IIR given in [9,19,20] as the time derivative of the instantaneous ionization probability inside the laser pulse:

$$W(t) = dP(t)/dt = (d/dt) \int |a_p(t)|^2 d\mathbf{p}. \quad (1)$$

Here  $a_p(t)$  is the instantaneous ionization amplitude which is obtained by projecting the solution of the time-dependent Schrödinger equation (TDSE) on the continuous eigenstates  $|p\rangle$  of the field-free Hamiltonian. Together with the bound states, they span the entire Hilbert space of this system. The particular choice of the boundary conditions for  $|p\rangle$  is not important as long as we conduct the momentum integration in Eq. (1). In the following, we will use the set of  $|p\rangle$  with the ingoing boundary condition [21].

\*igorivanov@ibs.re.kr

†A.Kheifets@anu.edu.au

‡kyungtaec@gist.ac.kr

For our purpose, it will be convenient to switch to the equivalent Heisenberg operator formulation. We take the Schrödinger projection operator  $\hat{Q}$  and cast it in the Heisenberg representation:

$$\hat{Q} = \int |\mathbf{p}\rangle\langle\mathbf{p}|, \quad \hat{Q}(t) = \hat{U}(0, t)\hat{Q}\hat{U}(t, 0). \quad (2)$$

Here  $\hat{U}(t, 0)$  is the time-evolution operator satisfying the equation

$$i\partial\hat{U}(t, 0)/\partial t = \hat{H}(t)\hat{U}(t, 0), \quad (3)$$

with the initial condition  $\hat{U}(0, 0) = \hat{I}$ . In Eq. (2)  $\hat{H}(t) = \hat{H}_0 + \hat{H}_{\text{int}}(t)$ ,  $\hat{H}_0 = \hat{\mathbf{p}}^2/2 - 1/r$ , and we use the length form  $\hat{H}_{\text{int}}(t) = \mathbf{E}(t) \cdot \mathbf{r}$  for the interaction Hamiltonian.

With the use of Eq. (2), the instantaneous ionization probability entering Eq. (1) can be written as  $P(t) = \langle\phi_0|\hat{Q}(t)|\phi_0\rangle$ . Here  $\phi_0$  is the bound state of the target atom which will be the ground state of hydrogen in the following. We will also use a shortcut  $\langle\hat{A}\rangle = \langle\phi_0|\hat{A}|\phi_0\rangle$  for any operator  $\hat{A}$  and omit  $\phi_0$  for the brevity of notations. For the IIR we then obtain

$$W(t) = \langle d\hat{Q}(t)/dt \rangle, \quad (4)$$

which is an expectation value of the Heisenberg operator  $\hat{W}(t) = d\hat{Q}(t)/dt$ , with  $\hat{Q}(t)$  being defined by Eq. (2). We may call  $\hat{W}(t)$  the IIR operator. Equation (4) is, of course, completely equivalent to Eq. (1), which was obtained in the Schrödinger representation. The Heisenberg representation, however, is very useful in that it allows us to calculate the expectation value of the operator  $\hat{W}(t)$  which, according to Eq. (4), gives us the IIR as a function of time within the laser pulse duration. In addition, the Heisenberg representation allows us to define, in a natural way, the autocorrelation functions for different operators. We employed this feature of the Heisenberg representation in our earlier work [22] to study autocorrelation functions for the coordinate and momentum operators for an atom in a laser field. This served as a quantum generalization of the SMM. Presently, we will be interested in the autocorrelation function for the operator  $\hat{W}(t)$ :

$$C(t_2, t_1) = \langle \hat{W}(t_2)\hat{W}(t_1) \rangle. \quad (5)$$

This function provides us with information about the correlation between the ionization events occurring at different times inside the laser pulse. A study of this correlation is the main goal of the present work.

We go back to the Schrödinger representation and rewrite Eq. (5) as

$$\begin{aligned} C(t_2, t_1) &= \langle \hat{W}(t_2)\hat{W}(t_1) \rangle = \frac{d}{dt_1} \frac{d}{dt_2} \langle \hat{Q}(t_2)\hat{Q}(t_1) \rangle \\ &= \frac{d}{dt_1} \frac{d}{dt_2} \langle \hat{U}(t_2, 0)\phi_0|\hat{Q}\hat{U}(t_2, t_1)\hat{Q}|\hat{U}(t_1, 0)\phi_0 \rangle. \end{aligned} \quad (6)$$

We evaluate this expression by propagating the TDSE starting from  $\Psi(0) = \phi_0$  on the interval  $(0, t_1)$ , thereby obtaining the state vector  $\Psi(t_1)$  at  $t = t_1$ . Acting with the (Schrödinger) operator  $\hat{Q}$ , defined by Eq. (2), on this vector gives us the wave function  $\Psi_1(t_1) = \hat{Q}\Psi(t_1)$ .  $\Psi_1(t_1)$  is further propagated on the interval  $(t_1, t_2)$ , yielding the wave function  $\Psi_1(t_2)$ , from which we obtain  $\Psi_2(t_2) = \hat{Q}\Psi_1(t_2)$ .  $\Psi_2(t_2)$  is projected on

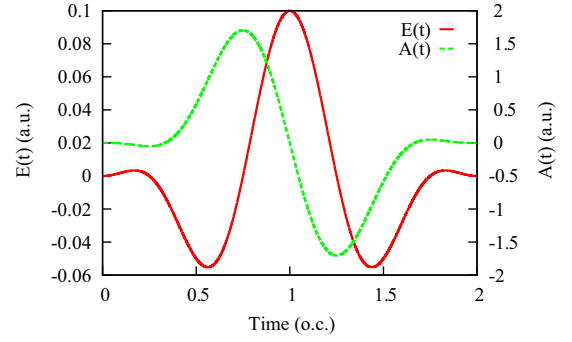


FIG. 1. Electric field and vector potential of the pulse (7) for  $\omega = 0.057$  a.u. and  $E_0 = 0.1$  a.u.

the state vector  $\Psi(t_2)$ , obtained by solving the TDSE with the initial condition  $\Psi(0) = \phi_0$  on the interval  $(0, t_2)$ . Finally, computing numerically the time derivatives as required by Eq. (6), we obtain the autocorrelation function.

To propagate the state vectors in time we use the numerical procedure [23] for the solution of the TDSE for the hydrogen atom driven by a laser pulse. In the present work we employ a linearly polarized laser pulse of the following form:

$$\mathbf{E}(t) = \hat{\mathbf{z}}E_0 \sin^2\{\pi t/T_1\} \cos \omega t, \quad (7)$$

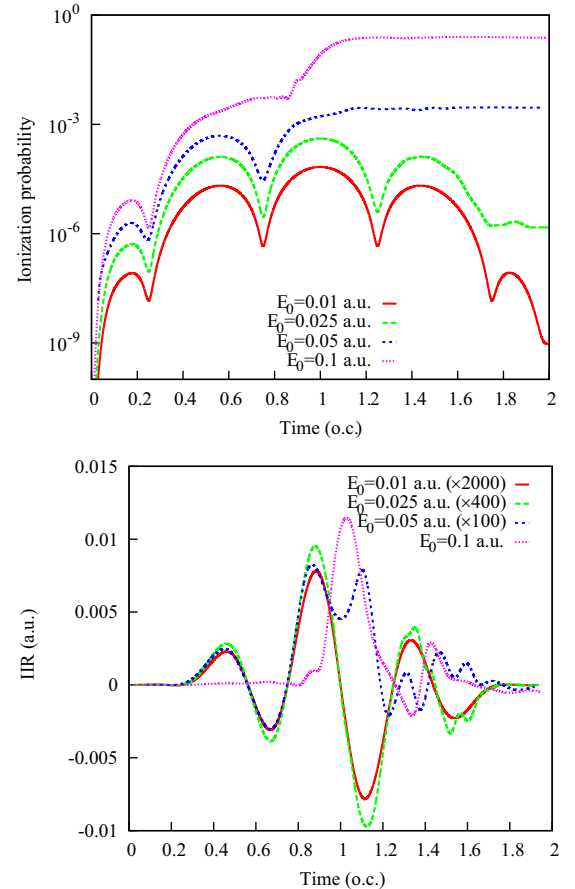


FIG. 2. Ionization probabilities and the IIRs obtained using Eq. (4) for different peak electric field strengths.

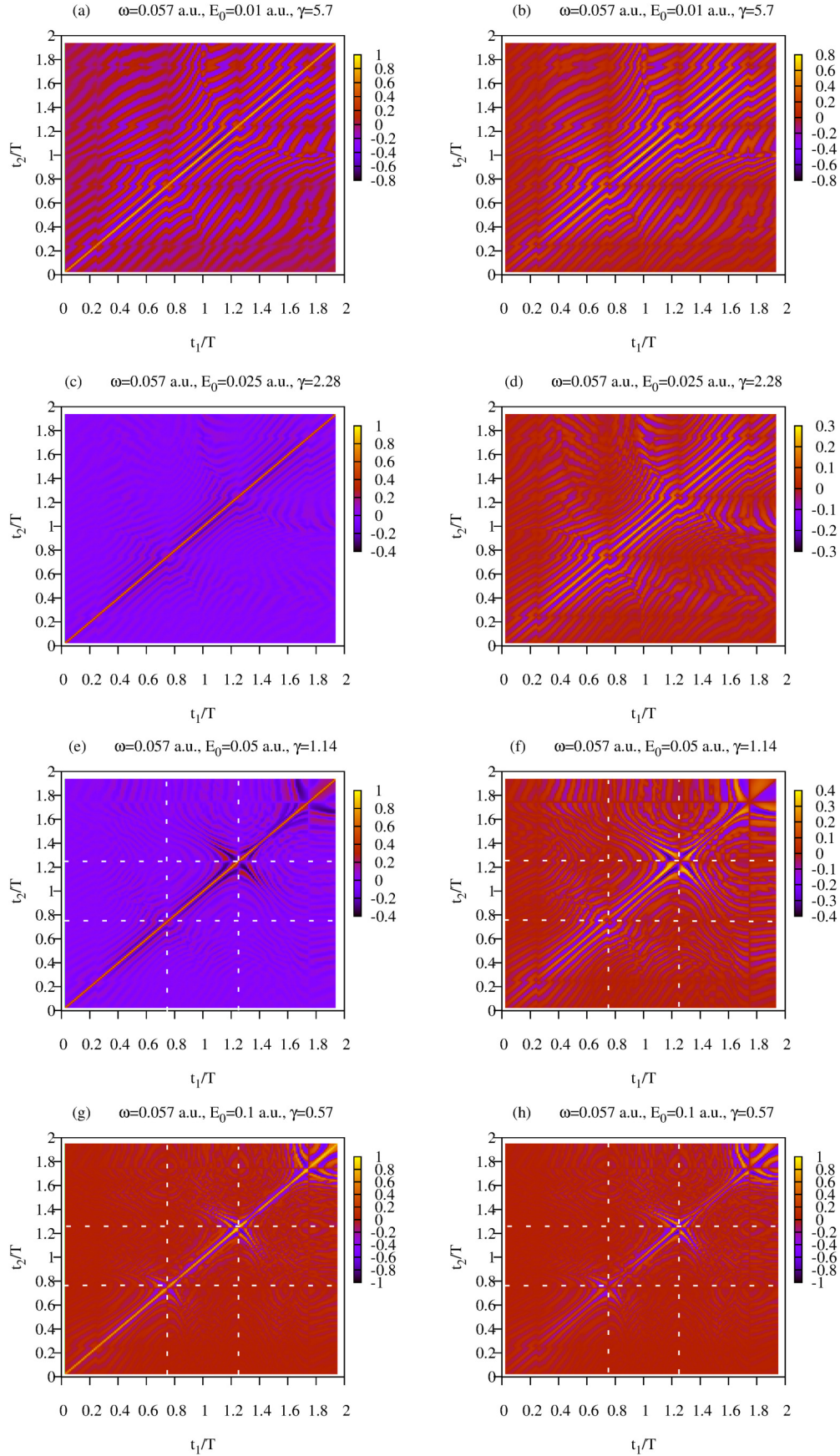


FIG. 3. Real (left) and imaginary (right) parts of the covariance function (9). For better visibility and to reveal more detail we plot the quantities,  $\text{Re}[\tilde{C}(t_1, t_2)]^{1/3}$  and  $\text{Im}[\tilde{C}(t_1, t_2)]^{1/3}$ . Dashed lines indicate extrema of the vector potential.

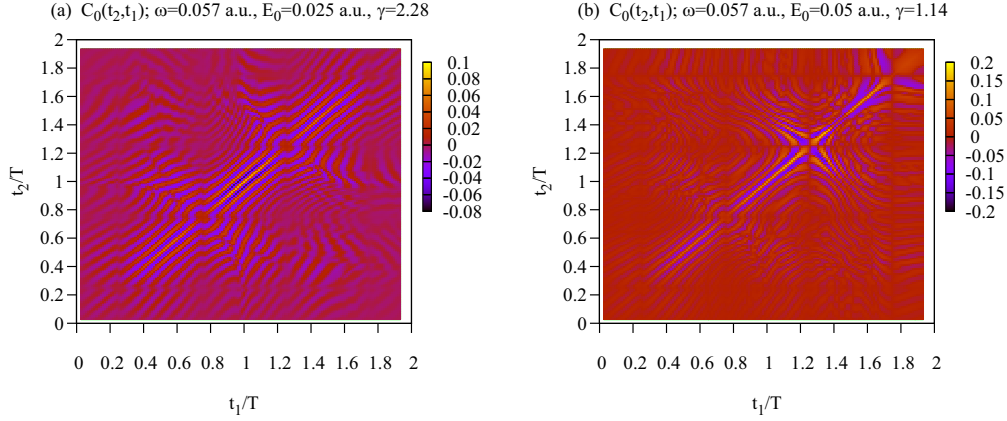


FIG. 4. Real part of the unnormalized covariance function (8) for different field strengths. For better visibility and to reveal more detail we plot  $\text{Re}[C(t_1, t_2)]^{1/3}$ .

with the peak field strength  $E_0$ , carrier frequency  $\omega$ , and total duration  $T_1 = 2T$ , where  $T = 2\pi/\omega$  is the optical cycle corresponding to the frequency  $\omega$ . In the following we will consider pulses with base frequency  $\omega = 0.057$  a.u. (corresponding to a wavelength of 800 nm) and different peak field strengths  $E_0$ . Figure 1 shows the shape of the pulse given by Eq. (7).

### III. RESULTS AND DISCUSSION

Results obtained from the TDSE solution for the instantaneous ionization probability and the IIR are shown in Fig. 2. Due to a high nonlinearity of the ionization process in the multiquantum ionization regime, the IIR varies considerably over the field strength range under consideration. This results in a strong variation of the magnitude of the autocorrelation function (5). To make a meaningful comparison of the role of correlation for different field strengths, we will consider the covariance function [24], which is closely related to the autocorrelation function (5). First, we define an autocorrelation function  $C_0(t_2, t_1)$ :

$$C_0(t_2, t_1) = \langle [\hat{W}(t_2) - W(t_2)][\hat{W}(t_1) - W(t_1)] \rangle. \quad (8)$$

Here  $W(t)$  is the expectation value of the time-dependent IIR operator  $\hat{W}(t) = d\hat{Q}(t)/dt$  in Eq. (4).  $C_0(t_2, t_1)$  provides a measure of the correlations between deviations from the expectation values of the IIR operator at different moments of time. Normalized  $C_0(t_2, t_1)$  gives the covariance function:

$$\tilde{C}(t_2, t_1) = \frac{C_0(t_2, t_1)}{\sqrt{C_0(t_1, t_1)C_0(t_2, t_2)}}. \quad (9)$$

This function is a more convenient indicator of the presence or lack of correlation at different instants of time. In particular [24], the zero value of the covariance function implies absence of any correlation, while  $|\tilde{C}(t_2, t_1)| \approx 1$  implies a strong correlation between the events at  $t_1$  and  $t_2$ . Results of the *ab initio* TDSE calculations of the real and imaginary parts of  $\tilde{C}(t_1, t_2)$  for different field strengths are shown in Fig. 3.

The interval of the field strengths selected in Fig. 3 covers both the multiphoton and tunneling ionization regimes. Expectedly, we see a dramatic difference between the correlation patterns in these two regimes. A strong correlation along the main diagonal line seen in both regimes is essentially trivial, reflecting only the fact that events occurring at the same

instant of time are strongly correlated. More interesting are the areas with  $t_1 \neq t_2$ . In the multiphoton regime [Figs. 3(a)–3(d) with  $\gamma = 2.28$  and 5.7] one can observe a strong correlation and anticorrelation densely filling the whole area of the plot. Lines of the constant elevation of the covariance function in this regime are, to a good approximation, straight lines  $t_1 - t_2 = \text{const}$ . Thus  $\tilde{C}(t_2, t_1)$  depends mainly on the difference in its arguments  $t_1 - t_2$ .

These features can be understood within the LOPT, which is valid in the multiphoton regime [25]. By introducing an expansion of the time-dependent wave function over the eigenvectors  $\phi_k$  of the field-free atomic Hamiltonian with energies  $\varepsilon_k$ ,  $\Psi(t) = \sum_k c_k(t)\phi_k e^{-i\varepsilon_k t}$ , we can express the autocorrelation function of the projection operator (2) as

$$\langle \hat{Q}(t_2)\hat{Q}(t_1) \rangle = \iint_{\varepsilon_{k_2} > 0, \varepsilon_{k_1} > 0} c_{k_2}^*(t_2)c_{k_1}(t_1) \times \langle \phi_{k_2} | \hat{U}(t_2, t_1) | \phi_{k_1} \rangle e^{i(\varepsilon_{k_2}t_2 - \varepsilon_{k_1}t_1)} dk_1 dk_2 \quad (10)$$

Within the LOPT, we can use the field-free evolution operator in Eq. (10), which leads to

$$\langle \hat{Q}(t_2)\hat{Q}(t_1) \rangle = \int_{\varepsilon_k > 0} c_k^*(t_2)c_k(t_1) dk. \quad (11)$$

The time dependence of the expansion coefficients is determined by a factor  $c_k(t) \propto \exp[i(\varepsilon_k - \varepsilon_0 - N\omega)t]$  [25]. Here  $N$  is the least number of photons the atom needs to absorb in order to be ionized.<sup>1</sup> The product of these factors in Eq. (11) will give us the correlation pattern depending on the time difference  $t_2 - t_1$  for the autocorrelation function (11) and consequently, by virtue of Eqs. (8) and (9), the same pattern for the covariance function.

When moving into the tunneling ionization regime [Figs. 3(e)–3(h) with  $\gamma = 1.14$  and 0.57] one encounters another type of correlation which manifests as the short segments of lines  $t_1 + t_2 = \text{const}$ , perpendicular to the main diagonal. This type of correlation gains its strength deeper

<sup>1</sup>Indeed, this factor, together with the corresponding energy denominator, leads to the Fermi golden rule in the limit  $t \rightarrow \infty$ .

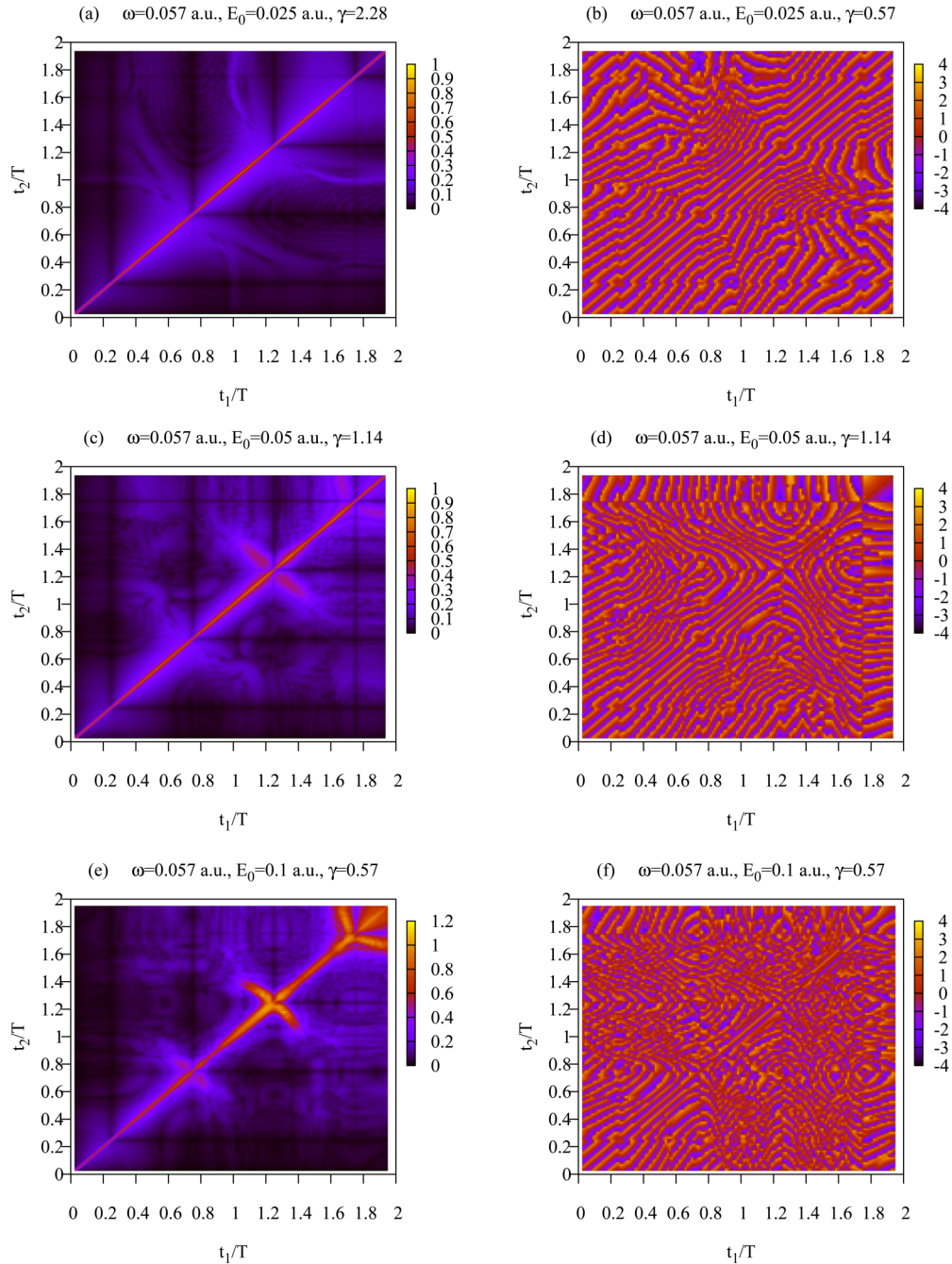


FIG. 5. Modulus (left) and argument (right) of the covariance function (9). For better visibility and to reveal more detail we plot the quantity  $|\tilde{C}(t_1, t_2)|^{1/3}$ .

into the tunneling ionization regime. For  $\gamma = 0.57$ , it becomes dominant, superseding almost entirely the correlation pattern present in the multiphoton regime. As one can observe from Fig. 1, the perpendicular lines appear near the extrema of the vector potential of the pulse [white dashed lines in Figs. 3(e)–3(h) show the positions of two extrema of the vector potential of the pulse (7) at  $t = 0.75T$  and  $t = 1.25T$ ]. The origin of these lines can be explained as follows using the simplified description of the ionization process provided by SMM. Let  $t_0$  be an extremum of the vector potential of the pulse. Then, for a small  $\tau$ , the vector po-

tential values at  $t_1 = t_0 - \tau$  and  $t_2 = t_0 + \tau$  are equal. Now we recall that in the SMM, which describes qualitatively the main features of tunneling ionization [10,26–29], the asymptotic electron velocities recorded at the detector are determined by the vector potential at the instant of ionization. These velocities are therefore equal for the ionization events occurring at  $t = t_1$  and  $t = t_2$ , provided electrons are emitted with zero initial velocities. The electron waves emitted at these instants shall thus interfere. As is well known, the interference process can be interpreted as the presence of correlation [24]. Since at  $t_0$  the electric field

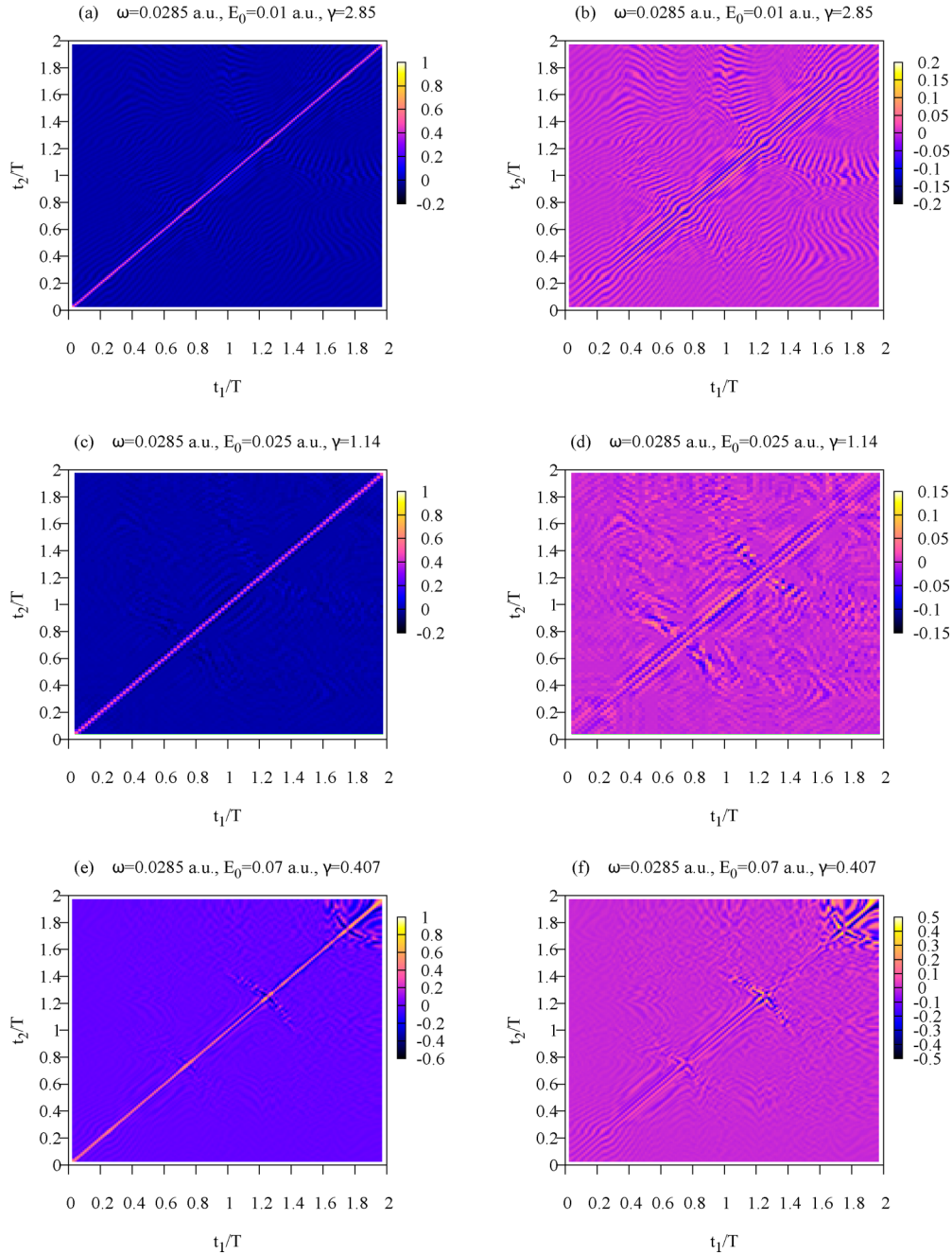
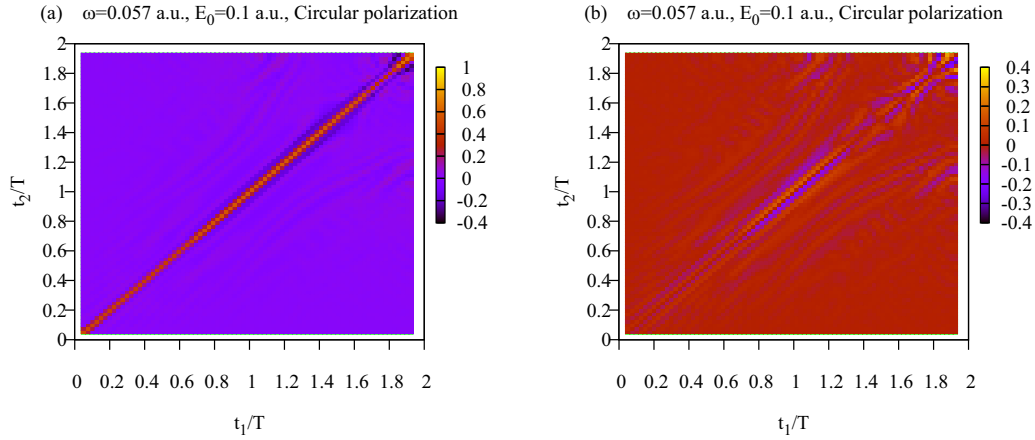


FIG. 6. Same as in Fig. 3 for the driving pulse wavelength  $\lambda = 1600$  nm.

passes through zero, the electrons are emitted on the opposite sides of the nucleus and can interfere constructively or destructively, depending on the phase the waves acquire during the subsequent motion. Destructive interference explains the anticorrelation stripe  $t_1 + t_2 = 2t_0$  in the plots for the real part of the correlation function running through the point  $(t_0, t_0)$  in Figs. 3(e) and 3(g) at  $t_0 = 1.25T$ . To account for the parallel nearby stripes of positive correlation, which can also be seen in Figs. 3(e) and 3(g), we can postulate (following the work [16]) that electrons emerge into the continuum with some initial velocity spread. One can see that such velocity spread in initial velocities and coordinates, leading to the different phases acquired by the electron waves during the

propagation, may lead to the observed interference patterns. This type of correlation pattern depends mainly on the sum  $t_1 + t_2 \approx 2t_0$ . It also weakens away from the main diagonal as  $\tau$  increases.

Figure 3 shows results for the normalized autocorrelation function  $\tilde{C}(t_2, t_1)$  defined in Eq. (9). That was done mainly for the sake of convenience of comparison so that autocorrelation functions for different ionization regimes varied in the same range. Had we used the unnormalized autocorrelation function  $C_0(t_2, t_1)$  defined in Eq. (8), we would arrive at the same conclusions about the presence of two mechanisms responsible for appearance of correlations in the multiphoton and tunneling regimes. To illustrate this point, we show in Fig. 4


 FIG. 7. Same as in Fig. 3 for circular polarized laser field at  $\lambda = 800$  nm.

the real part of the unnormalized autocorrelation function  $C_0(t_2, t_1)$  defined in Eq. (8) for different peak field strengths. These plots are to be compared with the plots shown in Figs. 3(c) and 3(e). We see that apart from the relatively trivial modifications [the unnormalized  $C_0(t_2, t_1)$  is, of course, driven to zero when its arguments approach the endpoints of the interval  $(0, 2T)$ , where field vanishes] and the change of the overall scale, data shown in Fig. 4 lead us to the same conclusions. In the multiphoton regime shown in Fig. 4(a) we see, just as in Fig. 3(c), a pattern of correlations with lines of constant elevation being, to a good approximation, straight lines  $t_1 - t_2 = \text{const}$ . When we approach the tunneling regime of ionization [Fig. 4(b)], we see a different pattern emerging which manifests itself, just in Fig. 3(e), as the short segments of lines  $t_1 + t_2 = \text{const}$  perpendicular to the main diagonal.

It might also be useful to look at the polar form representation of the normalized covariance function (9)  $\tilde{C}(t_2, t_1) = |\tilde{C}(t_1, t_2)|e^{i\theta(t_2, t_1)}$ . The modulus  $|\tilde{C}(t_1, t_2)|$  and argument  $\theta(t_2, t_1)$  are shown in Fig. 5. For the multiphoton regime in Figs. 5(a) and 5(b) the lines of the constant argument of  $\tilde{C}(t_2, t_1)$  are approximately straight lines parallel to the main diagonal, which agrees with the picture we obtained above using the LOPT. Indeed, we may expect in this case [using the same reasoning we relied on to obtain Eq. (11)] that the behavior of  $\tilde{C}(t_2, t_1)$  in the complex plane is largely mimicked

by the exponential function  $e^{i\alpha(t_1, t_2)(t_1 - t_2)}$  with some real and slowly varying function  $\alpha(t_1, t_2)$ . To a good approximation, the lines of the constant argument of  $\tilde{C}(t_2, t_1)$  in the  $(t_1, t_2)$  plane are therefore the lines  $t_1 - t_2 = \text{const}$ . When we move deeper into the tunneling regime shown in Figs. 5(c)–5(f), we again see gradual emergence of another type of correlation pattern pertaining to the tunneling regime of ionization, which we explained above invoking the SMM. In the polar form representation of  $\tilde{C}(t_2, t_1)$ , this type of correlation reveals itself through the appearance of the islands of large absolute magnitude of  $\tilde{C}(t_2, t_1)$  in the  $(t_1, t_2)$  plane. In agreement with the mechanism of appearance of correlations acting in the tunneling regime which we proposed above, these islands are stretched along the lines  $t_1 + t_2 = \text{const}$ , perpendicular to the main diagonal, and appear near the extrema of the vector potential of the pulse.

#### IV. UNIVERSALITY OF CORRELATIONS

An important question to address is how universal is the appearance of the correlations we described above? To be truly universal the main features of the observed correlation patterns should not depend on the particular pulse parameters we are using. Below we will try to answer this question of the

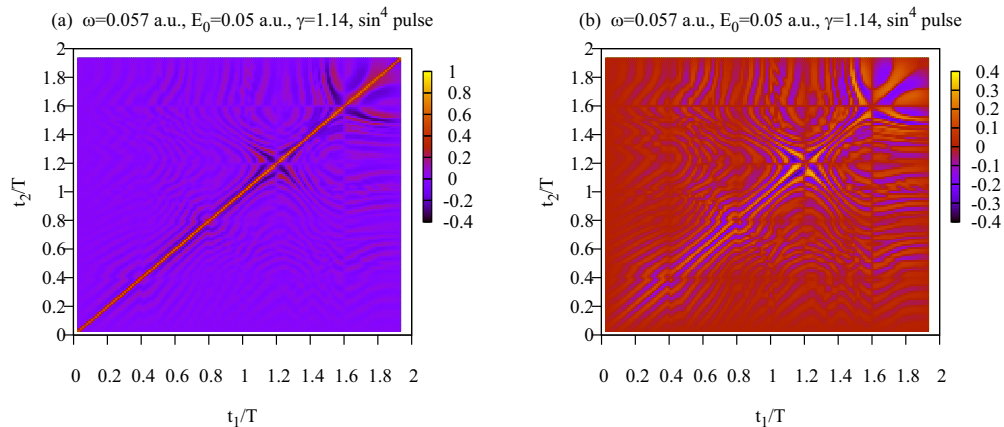


FIG. 8. Same as in Fig. 3 for the pulse (13).

universality of the correlations mechanism by analyzing the results obtained for different pulse parameters.

### A. Dependence on frequency

We first present results of the additional computations with the driving pulse at  $\lambda = 1600$  nm (photon frequency of  $\omega = 0.0285$  a.u.) using the same wave form (7) and total pulse duration of two optical cycles. For this wavelength of the driving pulse we selected field strengths varying from  $E_0 = 0.01$  to 0.07 atomic units. With the reduced photon energy the Keldysh parameter varied from  $\gamma = 2.85$  to 0.407, thus covering both the multiphoton and tunneling ionization regimes. Our results are shown in Fig. 6. One may observe the same pattern of time correlation changing from the parallel stripes  $t_1 - t_2 = \text{const}$  in the multiphoton to the perpendicular lines  $t_1 + t_2 = \text{const}$  in the tunneling regime. Hence, the main conclusion of the present article is sustained in this physically more transparent but computationally much more challenging regime.

### B. Polarization dependence

To corroborate in more detail the universality of the correlation mechanism in the most interesting tunneling regime, we have conducted an additional set of calculations with circular pulse propagating along the  $z$  direction and described by the following wave forms:

$$\begin{aligned} E_x(t) &= \frac{E_0}{\sqrt{2}} \sin^2 \{ \pi t / T_1 \} \cos \omega t, \\ E_y(t) &= \frac{E_0}{\sqrt{2}} \sin^2 \{ \pi t / T_1 \} \sin \omega t, \end{aligned} \quad (12)$$

with the peak field strength  $E_0 = 0.1$  a.u., total duration  $T_1 = 2T$ , where  $T = 2\pi/\omega$  is the optical cycle corresponding to the wavelength of 800 nm. The results presented in Fig. 7 show no sign of the correlations dependent on  $t_1 + t_2$  (the stripes perpendicular to the main diagonal). The reason for disappearance of this correlation is well understood within the original mechanism that we proposed in our paper. Indeed, the requirement  $A(t_1) = A(t_2)$  on which our mechanism of the appearance of correlations in the tunneling regime hinges can be satisfied by the vector potential in the linear polarization case near the extrema of  $A(t)$ . However, for the circular polarization, it cannot be satisfied for both components of the vector potential simultaneously. Therefore, the calculation for the circular polarization presents yet another confirmation of the mechanism we have proposed in our paper.

### C. Pulse shape dependence

We also checked the validity of the correlation mechanism we propose using different driving pulse shape and durations. We first present results obtained for the correlation function if instead of Eq. (7) the driving pulse is defined in terms of the vector potential:

$$E(t) = -\frac{\partial A(t)}{\partial t}, \quad A(t) = -\hat{z} \frac{E_0}{\omega} \sin^4 \{ \pi t / T_1 \} \sin \omega t. \quad (13)$$

Results are shown in Figs. 8 and 9. Figure 9 zooms on the correlation pattern near an extremum of the vector potential for two different pulse shapes: the pulse given by Eq. (7) and the pulse defined by Eq. (13). The extrema of the vector potential for both pulse shapes differ. Figure 9 shows that the correlation patterns shift accordingly, thereby confirming the

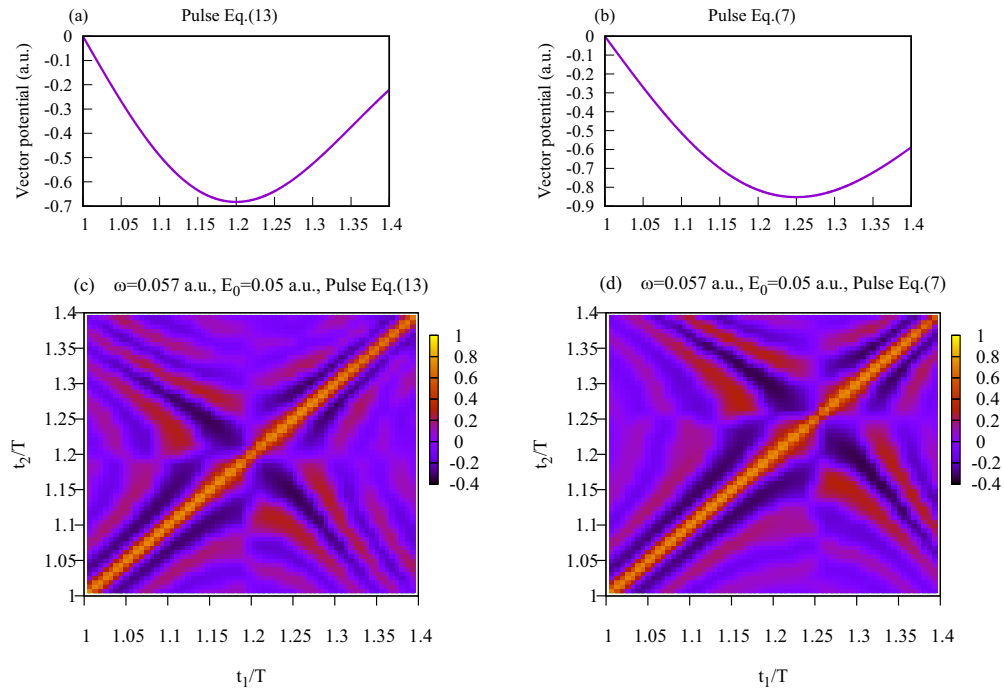


FIG. 9. Vector potential and the real part of the covariance function are displayed for the pulse (13) (left column) and the pulse defined by the electric field with the  $\sin^2$  envelope as in Eq. (7) (right column).

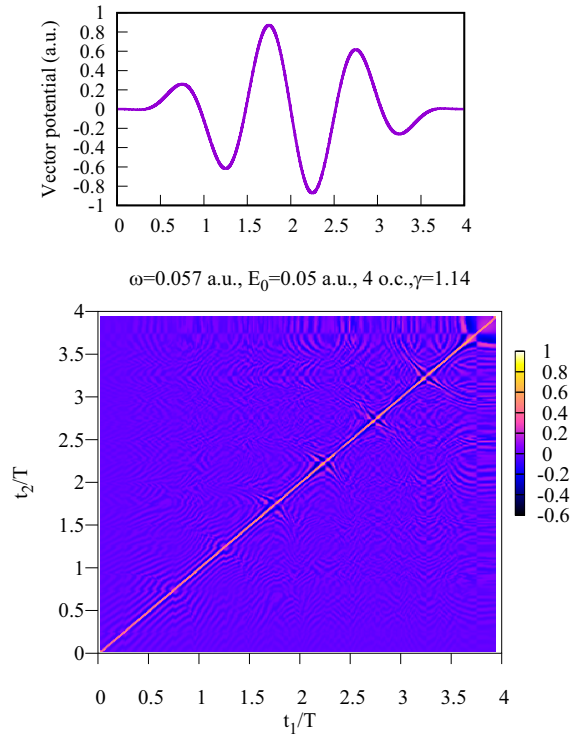


FIG. 10. Vector potential and the real part of the covariance function for the pulse (7) with total duration of four optical cycles. For better visibility and to reveal more detail, we plot the quantity  $\text{Re}[\tilde{C}(t_1, t_2)]^{1/3}$ .

universality of the mechanism of correlations we advocate in the paper.

Finally, Fig. 10 shows results obtained for the pulse given by Eq. (7) for the total pulse duration of four optical cycles corresponding to the base wavelength of  $\lambda = 800$  nm. This figure shows correlation patterns quite similar to those shown in Fig. 3. We can therefore state with confidence that the correlation patterns we discuss are not merely features due to the particular pulse parameters we are employing but rather have universal character.

## V. CONCLUSION

In conclusion, we performed the time-correlation analysis of strong-field ionization of atomic hydrogen driven by a nearly single-oscillation laser pulse. Our analysis covers the multiphoton regime  $\gamma \gg 1$  and the onset of the tunneling ionization regimes  $\gamma \leq 1$ . Both regimes manifest themselves by different time-correlation patterns. In the multiphoton regime, the strongest correlation occurs along the lines  $t_2 - t_1 = \text{const}$ . In the tunneling regime the correlation pattern is mainly determined by the sum  $t_1 + t_2$  near the vector potential extrema. Both type of correlations are readily explained by simple qualitative analysis based on the LOPT and SMM in the multiphoton and tunneling ionization regimes, respectively.

We hope that our pioneering investigation will prompt further theoretical studies of the variety of subcycle and intracycle interference phenomena. Given that the correlation function is, in principle, an experimentally measurable quantity [30], this approach may also offer the possibility of a new paradigm in the experimental studies of these phenomena. An experimental setup for such a study might be organized in a way similar to the one used in [31], where a short weak signal pulse (FWHM of 280 as) arriving with a variable delay with respect to the fundamental pulse was used to perturb the ionization process. Imposing such a perturbation disrupts the mechanism of correlations we described and should lead to measurable consequences. We ourselves are considering the process of strong-field ionization driven by circularly polarized pulses to correlate the number of absorbed photons at different instants within a single pulse or a sequence of several pulses. This analysis, which could open new possibilities for quantum local realism tests, will be presented elsewhere.

## ACKNOWLEDGMENTS

This work was supported by the Institute for Basic Science under Grant No. IBS-R012-D1. One of the authors (I.A.I.) wishes to thank the Australian National University for warm hospitality. Resources of the National Computational Infrastructure (NCI Australia) were employed.

- [1] A. Einstein, B. Podolsky, and N. Rosen, Can quantum-mechanical description of physical reality be considered complete? *Phys. Rev.* **47**, 777 (1935).
- [2] R. Hanbury Brown and R. Q. Twiss, A test of a new type of stellar interferometer on Sirius, *Nature (London)* **177**, 1046 (1956).
- [3] G. Goldhaber, W. B. Fowler, S. Goldhaber, T. F. Hoang, T. E. Kalogeropoulos, and W. M. Powell, Pion-Pion Correlations in Antiproton Annihilation Events, *Phys. Rev. Lett.* **3**, 181 (1959).
- [4] W. RuGway, A. G. Manning, S. S. Hodgman, R. G. Dall, A. G. Truscott, T. Lamberton, and K. V. Kheruntsyan, Observation of Transverse Bose-Einstein Condensation Via Hanbury Brown–Twiss Correlations, *Phys. Rev. Lett.* **111**, 093601 (2013).
- [5] N. Bohr, Can quantum-mechanical description of physical reality be considered complete? *Phys. Rev.* **48**, 696 (1935).
- [6] U. Fano, Quantum theory of interference effects in the mixing of light from phase-independent sources, *Am. J. Phys.* **29**, 539 (1961).
- [7] A. M. Perelomov, V. S. Popov, and M. V. Terentiev, Ionization of atoms in an alternating electric field, *Sov. Phys. -JETP* **23**, 924 (1966).
- [8] M. V. Ammosov, N. B. Delone, and V. P. Krainov, Tunnel ionization of complex atoms and of atomic ions in an alternating electromagnetic field, *Sov. Phys. JETP* **64**, 1191 (1986).
- [9] G. L. Yudin and M. Y. Ivanov, Nonadiabatic tunnel ionization: Looking inside a laser cycle, *Phys. Rev. A* **64**, 013409 (2001).
- [10] P. B. Corkum, Plasma Perspective on Strong Field Multiphoton Ionization, *Phys. Rev. Lett.* **71**, 1994 (1993).
- [11] K. J. Schafer, B. Yang, L. F. DiMauro, and K. C. Kulander, Above Threshold Ionization Beyond the High Harmonic Cutoff, *Phys. Rev. Lett.* **70**, 1599 (1993).

- [12] H. Ni, U. Saalman, and J.-M. Rost, Tunneling Ionization Time Resolved by Backpropagation, *Phys. Rev. Lett.* **117**, 023002 (2016).
- [13] A. S. Landsman, M. Weger, J. Maurer, R. Boge, A. Ludwig, S. Heuser, C. Cirelli, L. Gallmann, and U. Keller, Ultrafast resolution of tunneling delay time, *Optica* **1**, 343 (2014).
- [14] L. Torlina, F. Morales, J. Kaushal, I. Ivanov, A. Kheifets, A. Zielinski, A. Scrinzi, H. G. Muller, S. Sukiasyan, M. Ivanov *et al.*, Interpreting attoclock measurements of tunneling times, *Nat. Phys.* **11**, 503 (2015).
- [15] T. Zimmermann, S. Mishra, B. R. Doran, D. F. Gordon, and A. S. Landsman, Tunneling Time and Weak Measurement in Strong Field Ionization, *Phys. Rev. Lett.* **116**, 233603 (2016).
- [16] N. Camus, E. Yakaboylu, L. Fechner, M. Klaiber, M. Laux, Y. Mi, K. Z. Hatsagortsyan, T. Pfeifer, C. H. Keitel, and R. Moshhammer, Experimental Evidence for Wigner's Tunneling Time, *Phys. Rev. Lett.* **119**, 023201 (2017).
- [17] I. Ivanov, C. Hofmann, L. Ortmann, A. S. Landsman, C. H. Nam, and K. T. Kim, Instantaneous ionization rate as a functional derivative, *Commun. Phys.* **1**, 81 (2018).
- [18] A. S. Kheifets, The attoclock and the tunneling time debate, *J. Phys. B* **53**, 072001 (2020).
- [19] M. Yuan, P. Xin, T. Chu, and H. Liu, Exploring tunneling time by instantaneous ionization rate in strong-field ionization, *Opt. Express* **25**, 23493 (2017).
- [20] I. A. Ivanov, C. H. Nam, and K. T. Kim, Endpoint contribution to the instantaneous ionization rate for tunneling ionization, *Phys. Rev. A* **91**, 063404 (2015).
- [21] R. G. Newton, *Scattering Theory of Waves and Particles* (McGraw-Hill, New York, 1966), 2nd ed.
- [22] I. A. Ivanov and K. T. Kim, Simple man model in the Heisenberg picture, *Commun. Phys.* **3**, 7 (2020).
- [23] I. A. Ivanov, Evolution of the transverse photoelectron-momentum distribution for atomic ionization driven by a laser pulse with varying ellipticity, *Phys. Rev. A* **90**, 013418 (2014).
- [24] L. Mandel and E. Wolf, *Optical Coherence and Quantum Optics* (Cambridge University Press, Cambridge, England, 1995).
- [25] N. B. Delone and V. P. Krainov, *Multiphoton Processes in Atoms* (Springer-Verlag, Berlin, 1994).
- [26] M. Lewenstein, P. Balcou, M. Y. Ivanov, A. L'Huillier, and P. B. Corkum, Theory of high-harmonic generation by low-frequency laser fields, *Phys. Rev. A* **49**, 2117 (1994).
- [27] F. Krausz and M. Ivanov, Attosecond physics, *Rev. Mod. Phys.* **81**, 163 (2009).
- [28] N. I. Shvetsov-Shilovski, D. Dimitrovski, and L. B. Madsen, Ionization in elliptically polarized pulses: Multielectron polarization effects and asymmetry of photoelectron momentum distributions, *Phys. Rev. A* **85**, 023428 (2012).
- [29] D. G. Arbo, C. Lemell, S. Nagele, N. Camus, L. Fechner, A. Krupp, T. Pfeifer, S. D. Lopez, R. Moshhammer, and J. Burgdorfer, Ionization of argon by two-color laser pulses with coherent phase control, *Phys. Rev. A* **92**, 023402 (2015).
- [30] P. Urich, S. Castrignano, H. Uys, and M. Kastner, Noninvasive measurement of dynamic correlation functions, *Phys. Rev. A* **96**, 022127 (2017).
- [31] S. B. Park, K. Kim, W. Cho, S. I. Hwang, I. Ivanov, C. H. Nam, and K. T. Kim, Direct sampling of a light wave in air, *Optica* **5**, 402 (2018).